Title
Control of a twisted domain wall motion supported by topology

Journal
Journal of Applied Physics, 135(10)

ISSN
0021-8979

Authors
Kim, Seong Tae
Han, Hee-Sung
Im, Mi-Young
et al.

Publication Date
2024-03-14

DOI
10.1063/5.0187965

Peer reviewed

Wide controllability of a Twisted Domain Wall Motion Supported by Topology

Seong Tae Kim[1,2†], Hee-Sung Han[3,4†], Mi-Young Im[3], and Soong-Geun Je[1,2*]

[1]*Department of Physics, Chonnam National University, Gwangju 61186, Republic of Korea*

[2]*Center for Quantum Technologies, Chonnam National University, Gwangju 61186, Republic of Korea.*

[3]*Center for X-ray optics, Lawrence Berkeley National Laboratory, Berkeley, CA 94720, USA*

[4]*Department of Materials Science and Engineering, Korea National University of Transportation, Chungju 27479, Republic of Korea*

[†]These authors contributed equally: Seong Tae Kim, Hee-Sung Han

*E-mail: sg.je@jnu.ac.kr

Abstract

We report the topology-mediated modulation of a twisted domain wall speed in a thick perpendicularly magnetized system. By exploiting the topological robustness of the direction of the Bloch wall component in the twisted domain wall, we show that the domain wall speed either increases or decreases depending on whether the transverse magnetic field is parallel or antiparallel to the Bloch wall component. The decrease in the speed is maintained until the antiparallel transverse reaches ~0.3 T, indicating that the twisted domain wall can offer wide controllability supported by the topological robustness. We also demonstrate that the transverse magnetic field suppresses the Walker breakdown, allowing high mobility domain wall motion for a wide range of perpendicular driving fields.

I. Introduction

The ability to control magnetic domain wall (DW) motion enables the development of DW motion-based applications such as DW logic and memory devices [1,2]. So far, the DWs in an ultrathin system with perpendicular magnetic anisotropy have shown the most promising features in terms of mobility [3-6] as well as controllability [7-9]. Generally, the system consists of an ultrathin magnetic layer and heavy-metal layers, with strong spin-orbit interaction [10]. The DWs in such an effective two-dimensional system normally show the chiral Néel character, which is induced by the interfacial Dzyaloshinskii-Moriya interaction (DMI) [10-17]. For such chiral Néel DWs, the DW motion can be manipulated by applying in-plane magnetic fields which rotate the DW magnetization from the DMI-preferred direction [12-16]. The alteration from the preferred structure then leads to change in the DW energy, efficiency of the spin-torques, and/or chiral damping, resulting in the change of DW dynamics [18,19].

In the meantime, a three-dimensional DW structure in a multilayered magnetic system has attracted renewed interest in association with the realization of room-temperature magnetic skyrmions. Due to the increased influence of dipolar fields in the magnetic multilayers [20-23], stray-field skyrmion bubbles [24-26] with increased magnetic volume, can be stabilized at room temperature. Also, the dipolar field effect in a magnetic multilayered system or a thick ferrimagnetic system leads to an interesting topological DW structure, so-called the twisted DW, along the vertical dimension [21,26-29]. Figure 1(a) shows schematic illustrations of two ground states of the twisted DW. The circulating nature of the dipolar field tends to align the magnetizations on top and bottom surfaces to the opposite Néel configurations, forming the flux-closure magnetic configuration. It is interesting to note that the Néel configurations are stabilized even without the DMI. Also, continuously connecting the opposite Néel walls along the vertical direction requires 180° rotation of the magnetization with a Bloch wall component in the middle layer. Since there is no preferred sense of rotation, the Bloch wall component in the twisted DW can have either +*y* or -*y*-component with the same lowest energy level [21-26,30,31]. The side view (*i.e.* the *x-z* plane) of the twisted DW is analogous to the combination of the in-plane curling magnetization and vortex core of magnetic vortices, of which topology is characterized by the topological charge $Q = \int \mathrm{Q}_{\mathrm{dens}} \cdot \mathrm{d\,A} = \pm 1/2$ where Q_{dens}

$= \frac{1}{8}\epsilon^{ijk}\left[\mathrm{m}\cdot(\partial_i \mathrm{m}\times\partial_j \mathrm{m})\right]\cdot n$, where **m** is normalized magnetization vector, and **n** is surface normal vector [32-35]. Therefore, it can be expected that the twisted DW also shows the topology-originated unique static and dynamic properties such as topological robustness. Due to the non-trivial topology, once one of the Bloch wall components of the twisted DW is set, it is impossible to continuously reverse the Bloch wall component to the opposite direction.

The robustness of the Bloch wall component in the twisted DW then can provide an additional way of controlling the DW dynamics by applying a transverse magnetic field. As depicted in Fig. 1(b), when the transverse field B_y is parallel to the Bloch wall component, the twisted DW will be stable whereas the twisted DW will become unstable for antiparallel B_y. In a similar fashion to the asymmetric DW motion where an in-plane magnetic field modulates the DMI-preferred DW structure [13], this relative alignment between the Bloch wall component and B_y can lead to the variation of the dynamics of the twisted DW.

In this work, we study the influence of the transverse magnetic field B_y on the twisted DW motion using micromagnetic simulation. We find that, when the twisted DW is driven by a perpendicular magnetic field B_z, the DW speed either increases or decreases depending on whether B_y is parallel or antiparallel to the Bloch wall component of the twisted DW, respectively, allowing one to control the twisted DW motions. We reveal that, owing to the non-trivial topology of the twisted DW, the decreasing trend of the DW speed for the B_y antiparallel to the Bloch wall component is sustained for much stronger B_y that is a distinct feature from the case of the DW in the two-dimensional magnetic system. When the B_y is applied, the Walker breakdown is suppressed, thus enabling high mobility DW motion for a wide driving field range.

II. Methods

For this study, micromagnetic numerical simulations are performed using the Object Oriented MicroMagnetic Framework (OOMMF) software [36]. The OOMMF code yields the time evolution of the unit magnetization (m) in each simulation cell by solving the Landau-Lifshitz-Gilbert (LLG) equation [37,38], $\frac{d\mathrm{m}}{dt} = -|\gamma|\mathrm{m}\times \mathrm{B}_{\mathrm{eff}} + \alpha\,\mathrm{m}\times\frac{d\mathrm{m}}{dt}$, where γ is the gyromagnetic ratio, $\mathbf{B_{eff}}$ is the effective magnetic field, and α is the damping constant. $\mathbf{B_{eff}}$ includes all the fields coming from external magnetic fields, the uniaxial anisotropy, the demagnetizing effect, and the exchange interaction. Note that, to study the topological effect only by the dipolar fields, the DMI is excluded in our simulation. Material parameters used in the simulation are as follows [21,39]: saturation magnetization $M_s = 8 \times 10^5$ A/m, exchange stiffness constant $A_{ex} = 3.5 \times 10^{-11}$ J/m, uniaxial perpendicular anisotropy $K = 8 \times 10^5$ J/m^3, and Gilbert damping constant $\alpha = 0.5$. We employed a nanowire of the length $L = 2{,}000$ nm, the width $W = 200$ nm, and the thickness $h = 55$ nm. The thickness is about 9 times of the exchange length $l_{ex} = \sqrt{A_{ex}/K} = 6.614$ nm and the cell size is chosen to be $2.5 \times 2.5 \times 2.5$ nm^3, allowing the stabilization of the twisted DW with smoothly rotating magnetization along the vertical direction through 22 layers in twisted DW. With the simulation parameters, we successfully stabilized the twisted DW in the nanowire as shown in Fig. 1(b), and the Bloch wall component is initially aligned into the positive y-direction. One may assume that the twisted DW is stabilized in a thick magnetic system. However, it can occur in multilayered ultrathin magnetic films with multilayer repeats more than 3 [28].

III. Results

To investigate the dynamics of the twisted DW, we applied the transverse magnetic field B_y to induce the change in the DW speed during the motion of the twisted DW by $+B_z$ (Fig. 1(b)). The DW speed is measured by tracking the DW position as a function of time. The DW position is determined by fitting the m_z component along the x-axis with the function $m_z = \tanh((x-q)/\Delta)$ where q is the DW position and Δ is the average DW width of all the layers. Since the DW motion is affected by the ends of the nanowire, the DW motion near the middle of the nanowire is considered.

Figure 2(a) shows the moving distance of the DW as a function of time for parallel and antiparallel alignments of B_y. Note that the parallel B_y stands for $+B_y$ since the initial Bloch wall component is in the $+y$-direction. As the slope, *i.e.,* the DW speed, reflects, the application of B_y indeed modifies the speed of the twisted DW. The DW speed v_{DW} with respect to B_z for various values of B_y is summarized in Fig. 2(b). In the lower B_z regime, the v_{DW} increases linearly with B_z without experiencing dynamic deformation in the DW structure. Once the perpendicular magnetic field exceeds a threshold field, the v_{DW} suddenly drops followed by a linear increase with reduced mobility [3-5,40-45]. In the second linear regime, the twisted DW shows precessional motion. The sudden drop of the v_{DW} is so-called the Walker breakdown which is related to the onset of the precession of the DW magnetization. This behavior is previously shown in the current-driven motion of the twisted DW in multilayers [28]. In our simulations, this typical transition from the steady motion to the precessional motion is commonly observed for all values of B_y.

In the meantime, we found that the application of the B_y significantly modifies the v_{DW}. As shown in the zoomed image of the red box in Fig. 2(b), before the Walker breakdown, the positive B_y (dot symbols) increases the v_{DW} while the negative B_y (square symbol) decreases the v_{DW} which is in line with our motivation of this work. Interestingly, we also found that the application of the B_y suppresses the appearance of the Walker breakdown. Figure 2(c) indicates a threshold perpendicular magnetic field which triggers the Walker breakdown (B_{WB}). It clearly shows that as the positive B_y (circle dots) becomes stronger, the B_{WB} increases. That is, the B_y makes the steady motion region of DW structure be more widened, leading to the extension of the high mobility region to high magnetic fields.

The suppression of the Walker breakdown can qualitatively be understood by the stabilization of the DW structure by the application of B_y. In general, the driving force B_z tends to rotate the DW magnetization. As the rotation increases, the demagnetizing field effect inside the DW accordingly increases, resulting in a finite equilibrium tilt angle for the steady DW motion. Stronger B_z, however, allows the DW to overcome the energy barrier imposed by the DW demagnetizing fields, leading to the DW precession [44]. A similar behavior is also observed in a two-dimensional perpendicularly magnetized system in which the same stabilization mechanism is basically working [45]. In the twisted DW, it is observed that the precession first starts from the Bloch wall component in the middle layer where surface-volume stray field interaction is minimized [28]. Thus, the transverse field B_y can efficiently pin the Bloch wall component in the middle layer, inhibiting the Walker breakdown. Note that, in Fig. 2(c), the antiparallel B_y also suppresses the Walker breakdown. This result may seem counter-intuitive, however, we find that it is related to the reversal of the Bloch wall component prior to the Walker breakdown. This will be discussed in the subsequent parts.

To more clearly see the influence of the B_y on the twisted DW motion, we plotted the v_{DW}

for various values of B_z as a function of the transverse fields B_y as shown in Fig. 3(a). When the B_z is in the steady motion region ($B_z \leq 0.13$ T), the v_{DW} shows apparent B_y dependence: v_{DW} either increases or decreases depending on the direction of B_y that is in line with the result shown in Fig. 2(a). Interestingly, the decreasing trend of v_{DW} for negative B_y persists down to ~ −0.3 T, which is 15 % of the anisotropy field, for $B_z = 0.025$ T, indicating that the combination of the twisted DW and the transverse field B_y provides wide controllability of v_{DW}. Further increasing the magnitude of the negative B_y, leads to a sudden jump in the v_{DW}, which is related to the reversal of the Bloch wall component in the twisted DW as shown in Fig. 3(b). Once the Bloch wall component is reversed in the direction of the negative B_y, the situation becomes the same as the positive B_y case.

IV. Discussion

Such behaviors are unique to the twisted DW, which is obvious when compared to the DW in a two-dimensional plane. Figure 3(c) shows v_{DW} of a Bloch wall in a single layer with respect to B_y. Here, all the simulation parameters are identical to those of the twisted DW except that only single layer is taken for the Bloch wall case. Clearly, the v_{DW} is nearly independent of the sign of B_y in Fig. 3(c), meaning that the DW magnetization in the Bloch wall in the single layer is easily reversed by the B_y while the twisted DW structure is robust to the B_y. Meanwhile, there have been studies on the modulation of the DW speed by the transverse field [46-50]. However, these works focused on DWs in in-plane magnetized systems, and the range of the transverse field leading to the decrease in the DW speed is narrow. In this regard, our results on the twisted DW can be distinguished from the previous studies.

To understand the robustness of the twisted DW to the B_y, we investigated the detailed reversal mechanism of the Bloch wall component for $B_y = -0.3$ T and $B_z = 0.025$ T (Fig. 4(a)) along with the spatial distribution of Q_{dens} on surfaces in the three-dimensional system (Fig. 4(b)). The yellow and green surfaces indicate isosurface with $m_y \geq +0.9$ and $m_y \leq -0.9$, respectively. The initial Bloch wall component is aligned in the positive y-direction ($t = 0.00$ ns). Owing to its unique configuration analogous to the magnetic vortices, the initial Q of the twisted DW is not zero. Q_{dens} is localized on the right and left side surfaces with opposite signs due to the opposite direction of the surface normal vector as shown as color codes on the left and right sides in Fig. 4(a). This implies that the twisted DW contains the non-trivial topological spin texture.

As time passes, the initial Bloch components move towards the bottom surfaces of the medium while the twisted DW propagates in the x-direction. Interestingly, there is an asymmetry in the downward motion of the Bloch wall components. The Bloch wall component on the right urface is more shifted compared to that on the left surface. At t = 1.43 ns, the Bloch wall component on the right surface reaches the bottom surfaces. Subsequently, the Bloch wall component on the bottom surfaces moves in the $-y$-direction, and, simultaneously, the Bloch component with negative y-direction, start to emerge from the right surface (snapshot at t = 1.49 ns). The presence of these two opposite Bloch components results in more localized Q_{dens} on the bottom surface by forming the DW-skyrmion (red rectangle) which exhibits non-trivial topology [51-53]. The DW-skyrmion moves in the $-y$-direction (snapshot at t = 1.67 ns), and is suddenly annihilated by the injection of the Bloch point (magenta circle) (snapshot at t = 1.69 ns). The injection of the Bloch point indicates the discontinuous deformation which allows a break of continuity of the magnetization with sudden change in Q_{dens}. The formed Bloch point moves in the $-y$-direction with triggering the reversal of the Bloch component from the positive y-direction into the negative y-direction. As the Bloch point escapes through the left side surfaces, the Bloch wall component of the twisted DW is aligned in the negative y-direction.

The time-evolution of the topological charge Q of the twisted DW on each surface of the simulation region is also investigated. As shown in Fig. 4(b), the Q of the twisted DW was obtained by integrating of Q_{dens} over the top (Q_{top}, violet line), bottom ($Q_{bot.}$, dark yellow line), left ($Q_{lef.}$, orange line) and right ($Q_{rig.}$, green line) surfaces. It clearly shows that the formation of the DW-skyrmion on the bottom surface results in the decreases of Q_{rig} with involving the reversal of the Bloch component on the right surface (t ~ 1.49 ns).

To examine the role of the Bloch point during the reversal process, the summation of Q on all surfaces ($\Sigma Q_{surf.} = Q_{top}+Q_{bot.}+Q_{lef.}+Q_{rig.}$) was investigated (Fig.4(c)). It should be noted that $\Sigma Q_{surf.}$ is zero as long as there is no Bloch point within the simulation region. However, Fig. 4(c) shows that $\Sigma Q_{surf.}$ steeply increases and decreases. One can find that the initial increase of $\Sigma Q_{surf.}$ from zero to +1 is due to the change of Q_{bot} from -1 to 0. This is attributed to the transformation of the DW-skyrmion into the Bloch point on the bottom surface. $\Sigma Q_{surf.}$ then shows a sudden decrease to 0, which is resulted from the change of $Q_{lef.}$ by ΔQ ~ 1, signaling the escape of the Bloch point and the reversal of the Bloch wall component. from +*y*-direction to −*y*-direction.

Overall, the results in Fig. 4 show that, during the reversal process of the Bloch wall component of the twisted DW, the change in Q occurs and it is triggered by the nucleation and annihilation of the topologically non-trivial spin textures, i.e., the Bloch point and the DW-skyrmion. Since the formation of the topologically non-trivial spin textures occurs by overcoming a huge energy barrier dictated by the non-trivial topology [54, 55], one can conclude that the robustness of the twisted DW and, thus, the wide controllability of v_{DW} is attributed to the topology-originated energy barrier between the two twisted DWs having opposite Bloch components.

Note that in Fig. 3(a) the required transverse field B_y for the Bloch wall component reversal decreases as the B_z increases (dashed circle). This is related to the increasing destabilization of the twisted DW structure with B_z. As the twisted DW approaches the Walker breakdown with increasing B_z, reversing the Bloch wall component by the antiparallel B_y can be easily achieved. In Fig. 3(a), the Bloch wall component reversal in the twisted DW is accomplished prior to the onset of the Walker breakdown ($B_z \leq 0.13$ T, circle symbols). Thus, the Bloch wall component is already parallel to the negative B_y before the Walker breakdown. This explains why the negative B_y also suppresses the Walker breakdown, which is already mentioned in Fig. 2(c). Once the DW precession starts ($B_z > 0.13$ T, triangle symbols), there is no difference between positive and negative B_y cases, resulting in symmetric v_{DW} with respect to the $B_y = 0$ T as displayed in Fig. 3(a).

Finally, we provide qualitative understanding of the observed B_y dependence on v_{DW}. Although the twisted DW is too complex to be thoroughly explained by the one-dimensional DW model, the qualitative dynamics can be well understood using the one-dimensional model. In the one-dimensional model [44,45], the steady DW speed v_{DW} is proportional to the DW width Δ. We calculated the DW width Δ of the twisted DW with respect to the B_y at B_z = 0 T as displayed in Fig. 4. The Δ of the twisted DW is obtained by averaging values of Δ of each line profile. The parallel B_y (antiparallel B_y) results in broadening (narrowing) of the DW width Δ because that is the way of reducing the Zeeman energy. One can see that the Δ and v_{DW} with respect to B_y show a similar shape, indicating the relationship between the observed variation of v_{DW} and Δ by the transverse field B_y [45-50].

V. Conclusion

In summary, we investigated the influence of the B_y on the twisted DW motion using micromagnetic simulation. We found that, depending on whether B_y is parallel or antiparallel to the Bloch wall component of the twisted DW, the DW speed is either promoted or suppressed, enabling one to manipulate the twisted DW motion. Due to the topological nature of the twisted DW, remarkable controllability is obtained in a wide range of B_y (~ ±0.3 T), that is a distinct feature from that of the Bloch wall in a single magnetic layer. In addition, we found that the application of B_y can suppress the Walker breakdown of the twisted DW. The versatile controllability of the twisted DW dynamics thus points to utilization of the twisted DW for future DW motion based spintronic devices.

Acknowledgments

This work was supported by the National Research Foundation of Korea (NRF) grant funded by the Korea government (MSIT) (No. 2020R1C1C1006194). Works at LBNL were supported by U.S. Department of Energy (DE-AC02-05CH11231).

Data Availability

The data that support the findings of this study are available from the corresponding author upon reasonable request.

References

[1] D. A. Allwood, G. Xiong, C. C. Faulkner, D. Atkinson, D. Petit, and R. P. Cowburn, Magnetic Domain-Wall Logic, Science, **309**, 1688 (2005).

[2] S. S. P. Parkin, M. Hayashi, and L. Thomas, Magnetic domain-wall racetrack memory, Science, **320**, 190 (2008).

[3] R. Wieser, U. Nowak, and K. D. Usadel, Domain wall mobility in nanowires: Transverse versus vortex walls, Phys. Rev. B **69**, 064401(2004).

[4] J. Leliaert, B. Van de Wiele, A. Vansteenkiste, L. Laurson, G. Durin, L. Dupre, and B. Van Waeyenberge, Current-driven domain wall mobility in polycrystalline Permalloy nanowires: A numerical study, J. Appl. Phys. **115**, 233903 (2014).

[5] G. S. D. Beach, C. Nistor, C. Knutson, M. Tsoi, and J. L. Erskine, Dynamics of field-driven domain-wall propagation in ferromagnetic nanowires, Nat. Mater. **4**, 741 (2005).

[6] S. Konishi, S. Yamada, and T. Kusuda, Domain-wall velocity, mobility, and mean-free path in permalloy films, IEEE. Trans. Magn. **7**, 722 (1971).

[7] R. Skomski, H.-P. Oepen, and J. Kirschner, Micromagnetics of ultrathin films with perpendicular magnetic anisotropy. Phys. Rev. B **58**, 3223 (1998).

[8] T. A. Moore, I. M. Miron, G. Gaudin, G. Serret, S. Auffret, B. Rodmacq, A. Schuhl, S. Pizzini, J. Vogel, M. Bonfim, High domain wall velocities induced by current in ultrathin Pt/Co/AlOx wires with perpendicular magnetic anisotropy. Appl. Phys. Lett. **93**, 262504 (2008).

[9] I. Lemesh, F. Büttner, and G. S. D. Beach, Accurate model of the stripe domain phase of perpendicularly magnetized multilayers. Phys. Rev. B **95**, 174423 (2017).

[10] K.-S. Ryu, L. Thomas, S.-H. Yang, and S. S. P. Parkin, Chiral spin torque at magnetic domain walls. Nat. Nanotechnol. **8**, 527 (2013).

[11] K.-W. Kim, H.-W. Lee, K.-J. Lee, and M. D. Stiles, Chirality from interfacial spin–orbit coupling effects in magnetic bilayers. Phys. Rev. Lett. **111**, 216601 (2013).

[12] T. Koyama, D. Chiba, K. Ueda, K. Kondou, H. Tanigawa, S. Fukami, T. Suzuki, N. Ohshima, N. Ishiwata, Y. Nakatani, K. Kobayashi, and T. Ono, Observation of the intrinsic

pinning of a magnetic domain wall in a ferromagnetic nanowire, Nat. Mater. **10**, 194 (2011).

[13] S.-G. Je, D.-H. Kim, S.-C. Yoo, B.-C. Min, K.-J. Lee, and S.-B. Choe, Asymmetric magnetic domain-wall motion by the Dzyaloshinskii-Moriya interaction, Phys. Rev. B **88**, 214401 (2013).

[14] O. Boulle, S. Rohart, L. D. Buda-Prejbeanu, E. Jué, I. M. Miron, S. Pizzini, J. Vogel, G. Gaudin, and A. Thiaville, Domain Wall Tilting in the Presence of the Dzyaloshinskii-Moriya Interaction in Out-of-Plane Magnetized Magnetic Nanotracks, Phys. Rev. Lett. **111**, 217203 (2013).

[15] Y. Yoshimura, K.-J. Kim, T. Taniguchi, T. Tono, K. Ueda, R. Hiramatsu, T. Moriyama, K. Yamada, Y. Nakatani, and T. Ono, Soliton-like magnetic domain wall motion induced by the interfacial Dzyaloshinskii–Moriya interaction, Nat. Phys. **12**, 157 (2016).

[16] K. Shahbazi, J.-V. Kim, H. T. Nembach, J. M. Shaw, A. Bischof, M. D. Rossell, V. Jeudy, T. A. Moore, and C. H. Marrows, Domain-wall motion and interfacial Dzyaloshinskii-Moriya interactions in Pt/Co/Ir (t_{Ir})/Ta multilayers, Phys. Rev. B **99**, 094409 (2019).

[17] S. Emori, U. Bauer, S.-M. Ahn, E. Martinez, and G. S. D. Beach, Current-driven dynamics of chiral ferromagnetic domain walls. Nat. Mater. **12**, 611 (2013).

[18] E. Jué, C. K. Safeer, M. Drouard, A. Lopez, P. Balint, L. B.-Prejbeanu, O. Boulle, S. Auffret, A. Schuhl, A. Manchon, I. M. Miron, and G. Gaudin, Chiral damping of magnetic domain walls, Nat. Mater. **15**, 272 (2016).

[19] C. A. Akosa, I. M. Miron, G. Gaudin, and A. Manchon, Phenomenology of chiral damping in noncentrosymmetric magnets, Phys. Rev. B **93**, 214429 (2016).

[20] W. Legrand, J. Yves Chauleau, D. MacCariello, N. Reyren, S. Collin, K. Bouzehouane, N. Jaouen, V. Cros, and A. Fert, Hybrid chiral domain walls and skyrmions in magnetic multilayers, Sci. Adv. **4**, eaat0415 (2018).

[21] S. A. Montoya, S. Couture, J. J. Chess, J. C. T. Lee, N. Kent, D. Henze, S. K. Sinha, M.-Y. Im, S. D. Kevan, P. Fischer, B. J. McMorran, V. Lomakin, S. Roy, and E. E. Fullerton, Tailoring magnetic energies to form dipole skyrmions and skyrmion lattices, Phys. Rev. B **95,** 024415 (2017).

[22] F. Büttner, I. Lemesh, and G. S. D. Beach, Theory of isolated magnetic skyrmions: From fundamentals to room temperature applications, Sci. Rep. **8**, 4464 (2018).

[23] M. Schott, A. Bernand-Mantel, L. Ranno, S. Pizzini, J. Vogel, H. Béa, C. Baraduc, S. Auffret, G. Gaudin, and D. Givord, The Skyrmion Switch: Turning Magnetic Skyrmion Bubbles on and off with an Electric Field, Nano Lett. **17**, 3006 (2017).

[24] W. Jiang, P. Upadhyaya, W. Zhang, G. Yu, M. B. Jungfleisch, F. Y. Fradin, J. E. Pearson, Y. Tserkovnyak, K. L. Wang, O. Heinonen, S. G. E. te Velthuis, and A. Hoffmann, Blowing magnetic skyrmion bubbles, Science, **349**, 283 (2015).

[25] Y. Yao, B. Ding, J. Liang, H. Li, X. Shen, R. Yu, and W. Wang, Chirality flips of skyrmion bubbles, Nat. Commun. **13**, 5991 (2022).

[26] E. Schlömann, Twisted domain wall structure in bubble films, Appl. Phys. Lett. **21**, 227 (1972).

[27] I. Lemesh and G. S. D. Beach, Twisted domain walls and skyrmions in perpendicularly magnetized multilayers, Phys. Rev. B **98**, 104402 (2018).

[28] I. Lemesh and G. S. D. Beach, Walker Breakdown with a Twist: Dynamics of Multilayer Domain Walls and Skyrmions Driven by Spin-Orbit Torque. Phys. Rev. Appl. **12**, 044031 (2019).

[29] Y. Li, S. Mankovsky, S. Polesya, H. Ebert, and C. Moutafis, Magnetic Bloch-point hopping in multilayer skyrmions and associated emergent electromagnetic signatures, Phys. Rev. B **104,** L140409 (2021).

[30] L. Neel, Energie des parois de Bloch dans les couches minces, Comptes Rendus Hebdomadaires Des Seances De L Academie Des Sciences **241**, 533 (1955).

[31] N. L. Schryer, and L. R. Walker, The motion of 180° domain walls in uniform dc magnetic fields. J. Appl. Phys. **45**, 5406 (1974).

[32] H.-S. Han, S. Lee, M.-S. Jung, N. Kim, D.-H. Jung, M. Kang, H.-J. Ok, W. Chao, Y.-S. Yu, J.-I. Hong, M.-Y. Im, and K.-S. Lee, Tuning of oscillation modes by controlling dimensionality of spin structures, NPG Asia Mater. **14,** 91 (2022).

[33] N. Nagaosa and Y. Tokura, Topological properties and dynamics of magnetic skyrmions, Nat. Nanotechnol. **8**, 899 (2013).

[34] H.-B. Braun, Topological effects in nanomagnetism: from superparamagnetism to chiral quantum solitons, Adv. Phys. **61**, 1 (2012).

[35] H.-S. Han, S. Lee, D.-H. Jung, M. Kang, and K.-S. Lee, Chirality-dependent asymmetric vortex core structures in a harmonic excitation mode, Appl. Phys. Lett. **117**, 042401 (2020).

[36] M. J. Donahue and D. G. Porter, OOMMF code (see http://math.nist.gov/ oommf).

[37] T. L. Gilbert, A Lagrangian formulation of the gyromagnetic equation of the magnetization field, Phys. Rev. **100**, 1243 (1955).

[38] L. Landau and E. Lifshitz, On the Theory of the Dispersion of Magnetic Permeability in Ferromagnetic Bodies, Phys. Z. Sowjetunion **8**, 153 (1935).

[39] K. Niitsu, Temperature dependence of magnetic exchange stiffness in iron and nickel, J. Phys. D: Appl. Phys. **53**, 39LT01 (2020).

[40] J. Linder and M. Alidoust, Asymmetric ferromagnetic resonance, universal Walker breakdown, and counterflow domain wall motion in the presence of multiple spin-orbit torques, Phys. Rev. B **88**, 064420 (2013).

[41] K.-J. Kim, Y. Yoshimura, T. Okuno, T. Moriyama, S.-W. Lee, K.-J. Lee, Y. Nakatani, and T. Ono, Observation of asymmetry in domain wall velocity under transverse magnetic field, Apl. Mater. **4**, 032504 (2016).

[42] S.-K. Kim, J.-Y. Lee, Y.-S. Choi, K.Y. Guslienko, and K.-S. Lee, Underlying mechanism of domain-wall motions in soft magnetic thin-film nanostripes beyond the velocity-breakdown regime, Appl. Phys. Lett. **93**, 052503 (2008).

[43] J.-Y. Lee, K.-S. Lee, and S.-K. Kim, Remarkable enhancement of domain-wall velocity in magnetic nanostripes, Appl. Phys. Lett. **91**, 122513 (2007).

[44] A. Mougin, M. Cormier, J. P. Adam, P. J. Metaxas, and J. Ferré, Domain wall mobility, stability and Walker breakdown in magnetic nanowires, Europhys. Lett. **78**, 57007 (2007).

[45] O. Boulle, L. D. Buda-Prejbeanu, M. Miron, and G. Gaudin, Current induced domain wall dynamics in the presence of a transverse magnetic field in out-of-plane magnetized materials, J. Appl. Phys. **112**, 053901 (2012).

[46] J. Lu, X. R. Wang, Motion of transverse domain walls in thin magnetic nanostrips under transverse magnetic fields, J. Appl. Phys. **107**, 083915 (2010).

[47] M. T. Bryan, T. Schrefl, D. Atkinson, and D. A. Allwood, Magnetic domain wall propagation in nanowires under transverse magnetic fields, J. Appl. Phys. **103**, 073906 (2008).

[48] C.-Y. You, Equation of motion for a domain wall movement under a nonuniform transverse magnetic field, Appl. Phys. Lett. **92**, 192514 (2008).

[49] S. Glathe, I. Berkov, T. Mikolajick, and R. Mattheis, Experimental study of domain wall motion in long nanostrips under the influence of a transverse field, Appl. Phys. Lett. **93**, 162505 (2008).

[50] Y. Jang, S. Yoon, S. Lee, K. Lee, and B. K. Cho, Manipulating magnetic moment in a magnetic domain wall under transverse magnetic fields near Walker threshold, J. Appl. Phys. **108**, 063904 (2010).

[51] R. Cheng, M. Li, A. Sapkota, A. Rai, A. Pokhrel, T. Mewes, C. Mewes, D. Xiao, M. De Graef, and V. Sokalski, Magnetic domain wall skyrmions, Phys. Rev. B **99**, 184412 (2019).

[52] V. M. Kuchkin, B. Barton-Singer, F. N. Rybakov, S. Blügel, B. J. Schroers, and N. S. Kiselev, Magnetic skyrmions, chiral kinks, and holomorphic functions, Phys. Rev. B **102**, 144422 (2020).

[53] S. U. Han, W. Kim, S. K. Kim, and S.-G. Je, Tunable domain-wall skyrmion Hall effect driven by a current and a magnetic field, Phys. Rev. B **109**, 014404 (2024).

[54] H.-S. Han, S. Lee, M.-S. Jung, N. Kim, W. Chao, Y.-S. Yu, J.-I. Hong, K.-S. Lee, and M.-Y. Im, Topology-dependent stability of vortex-antivortex structures, Appl. Phys. Lett **118**, 212407 (2021).

[55] O. A. Tretiakov, and O. Tchernyshyov, Vortices in thin ferromagnetic films and the skyrmion number, Phys. Rev. B **75**, 012408 (2007).

Figures

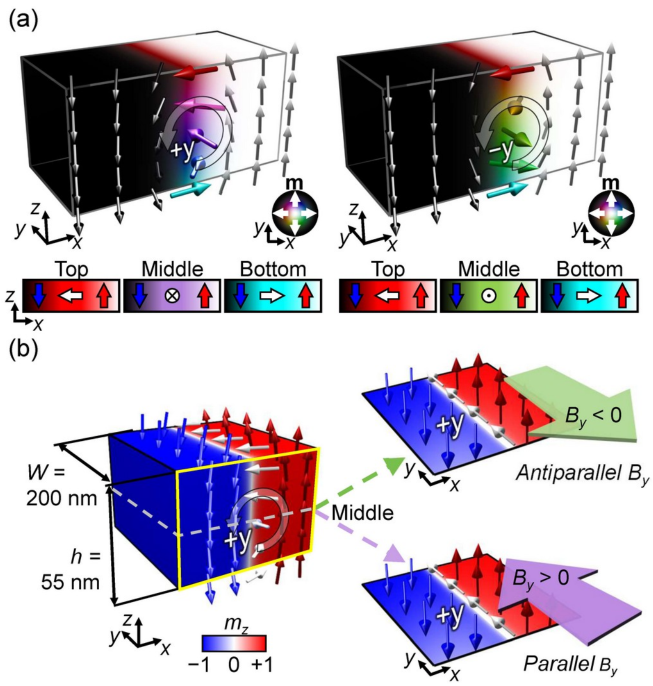

FIG. 1. (a) Schematic illustrations of the two twisted DWs with different Bloch wall component in the middle layer. (b) Conceptual diagram of the simulations along with the simulation dimensions.

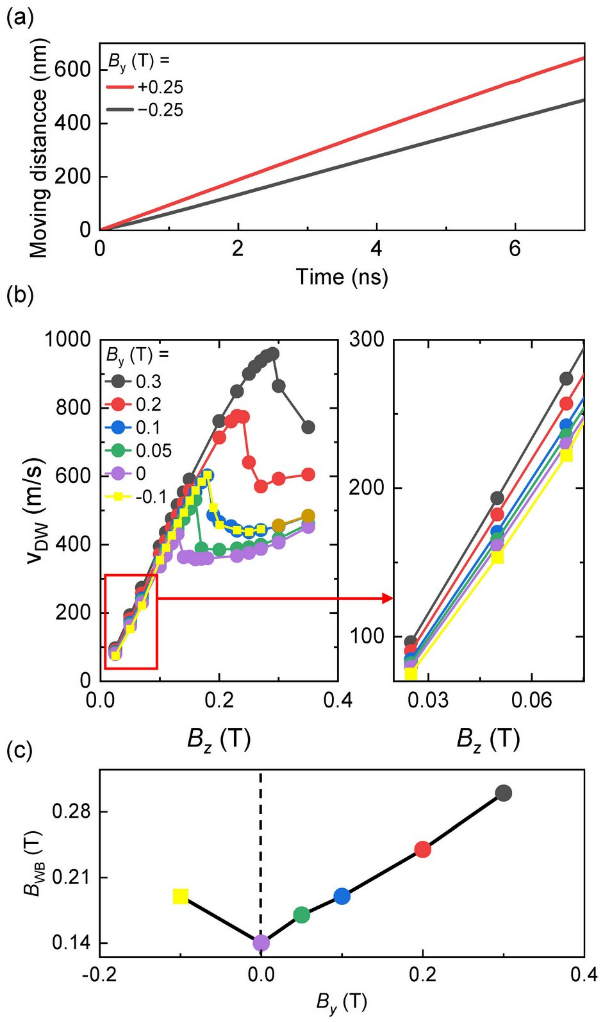

FIG. 2. (a) The moving distance of the twisted DWs as a function of the time for B_y = +0.25 T (red line) and −0.25 T (black line). The slope indicates the DW speed v_{DW}. (b) v_{DW} with respect to B_z for various B_y. The enlarged figure more clearly illustrates the speed difference in the steady motion region. (c) Threshold perpendicular magnetic field B_{WB} as a function of B_y.

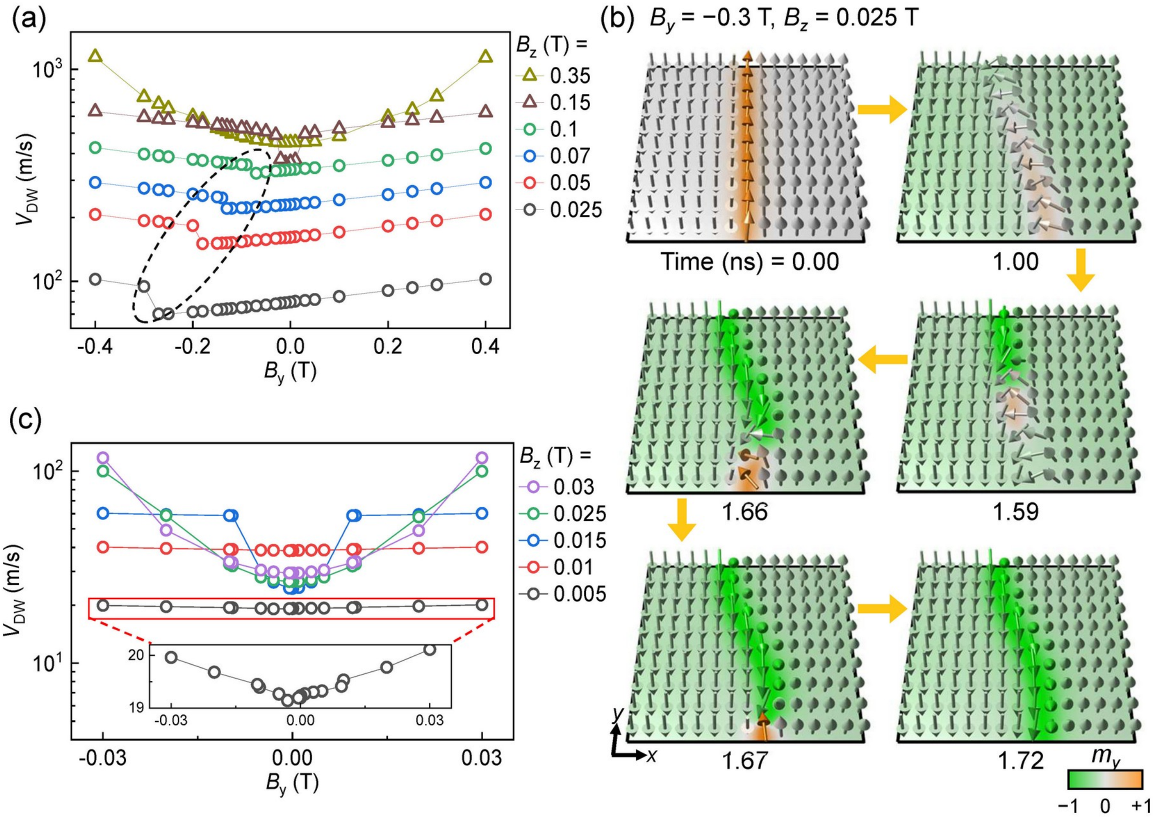

FIG. 3. (a) The DW speed v_{DW} of the twisted DW with respect to B_y for various values of B_z. (b) Snapshots of the magnetization configuration in the middle layer during the field-driven twisted DW motion for B_y = –0.3 T and B_z = 0.025 T. The color indicates m_y. (c) v_{DW} of the Bloch wall in a two-dimensional system with respect to the B_y for various values of B_z.

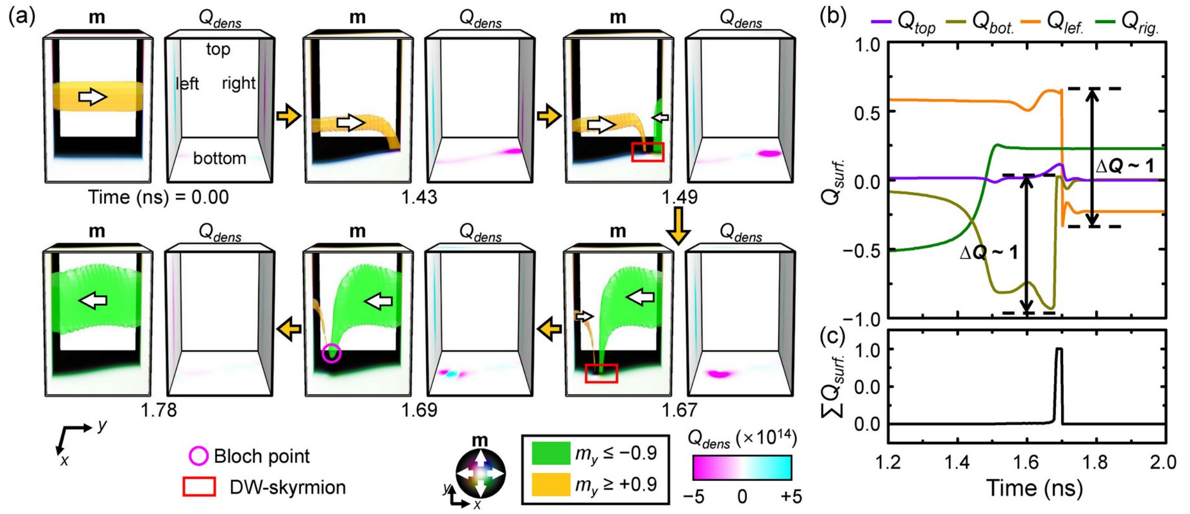

FIG. 4. (a) Three-dimensional visualization of the magnetization configurations of twisted DW (left) and spatial distribution of Q_{dens} over surfaces of medium (right). The yellow and green surfaces indicate isosurfaces with $m_y \geq +0.9$ and $m_y \leq -0.9$, respectively. (b) The time-evolution of the topological charge Q on surfaces of medium and (c) the summation of Q on all surfaces of medium $\Sigma Q_{surf.} = Q_{top}+Q_{bot.}+Q_{lef.}+Q_{rig.}$.

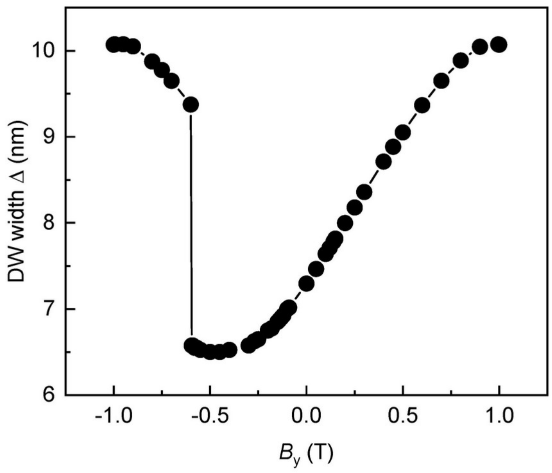

FIG. 5. The DW width as a function of the transverse field. The DW width is calculated for $B_z = 0$ T.